



## Research paper

Alpha-fluorescence ( $\alpha S_1$ ) from thermally stable carbon nanodotsRachel D. Schmitz<sup>a,b,1</sup>, Rachael Knoblauch<sup>a</sup>, Estelle Ra<sup>a</sup>, Chris D. Geddes<sup>a,\*</sup><sup>a</sup> Institute of Fluorescence, Department of Chemistry and Biochemistry, University of Maryland Baltimore County, Baltimore, MD 21202, USA<sup>b</sup> Lantham BioPharm Group, 701 East Pratt St, Suite 5047, Baltimore, MD 21202, USA

## HIGHLIGHTS

- A one-step combustion-based method yields alpha-fluorescent ( $\alpha S_1$ ) carbon nanodots.
- The nanodots show temperature-dependent  $\alpha S_1$  from aggregation in water.
- $\alpha S_1$  is observed without additional bond rigidification or fixation in solid media.
- Nanodot emission is stable over many heating-cooling and excitation-emission cycles.

## A B S T R A C T

Fluorescence from carbon nanodots has been of keen interest over the past decade; however, exploration of radiative pathways including delayed fluorescence ( $\alpha S_1$ ) from nanodots have *hitherto* seen little investigation, thus limiting the scope of nanodot applications. Simple synthesis strategies for  $\alpha S_1$ -emitting nanodots therefore remain necessary. Herein we report an inexpensive, quasi-spherical nanodot structure from combustion-based synthesis exhibiting strong excitation-dependent  $\alpha S_1$  emission upon aggregation to 100 nm sizes. Interestingly,  $\alpha S_1$  emission intensity is found to increase with increased temperature. The nanodots also exhibit photostability over multiple heating and cooling cycles, suggesting the possible use of these carbon nanodots as temperature-sensitive luminescence probes.

Carbon nanodots have been the focus of much research in recent years due to their intriguing photophysical properties and diversity of applications as fluorescent nanoparticles [1–3]. Carbon nanodots have not only been shown to be photostable; they have also demonstrated thermal and long-term dark stability [4,5]. Samples have been shown to absorb across the ultraviolet (UV) and visible range for a multitude of emission wavelengths and subsequent applications, with emissive properties arising from multiple internal fluorophores including varying surface trap states, multiple conjugated pi systems, and size-dependent quantum confinement [1,3,6]. These particles are organic with hydrophilic surface moieties that permit facile modification and biocompatibility for potential biomedical applications and imaging [3]. Despite their numerous advantages, to date the primary investigation of carbon nanodots has been on development solely for fluorescence applications; however there has been increased investigation into additional radiative pathways, such as phosphorescence ( $T_1 \rightarrow S_0$ ) [7–9] and delayed fluorescence ( $\alpha S_1 \rightarrow S_0$ ) [10–12], in recent years [13,14]. Delayed fluorescence, also referred to as alpha fluorescence ( $\alpha S_1$ ), is reported herein. This phenomenon is also commonly referred to as thermally activated delayed fluorescence (TADF) [10,12–14]. In  $T_1$  and  $\alpha S_1$  emission, an electron in the excited singlet state performs a spin flip to

occupy a triplet excited state of comparable energy through a process known as intersystem crossing (ISC,  $S_1 \rightarrow T_1$ ). The rate of this transition is most often relatively slow, yielding much longer radiative lifetimes of alpha fluorescence and phosphorescence—generally on the scale of micro- to milli-seconds—as compared to those of classical fluorescence, which typically occur in nanoseconds [15]. This leads to a characteristic “after-glow” for long-lived emission processes after the excitation source has ceased. Subsequently, triplet states are typically quenched by molecular species in solution such as molecular oxygen; thus, phosphorescence or  $\alpha S_1$  are *seldomly* detected in carbon nanodots at room temperature. Under these conditions, only fluorescence from the particles can be detected. When heat is applied to the system, however, the electron may undergo a reverse spin flip before the  $T_1$  excited state is quenched in a process known as reverse intersystem crossing (RISC,  $T_1 \rightarrow S_1$ ) and occupy its previous excited singlet state for eventual alpha fluorescence. This provides an alternative to quenching and can remarkably result in increased detected fluorescence intensity at higher temperatures [15]. The long lifetimes of alpha fluorescence permit exclusive collection of these signals by using an off-gated detection method that is ideal for clearer biological imaging, generating spectra that are free from background due to short-lived biological

\* Corresponding author.

E-mail address: [geddes@umbc.edu](mailto:geddes@umbc.edu) (C.D. Geddes).<sup>1</sup> This research was performed while Dr. Rachel D. Schmitz was at the Institute of Fluorescence, Baltimore, MD 21202, USA.

autofluorescence. The temperature dependence also permits  $\alpha S_1$  probes to act as temperature sensors for other applications. To date, only a very few reports of  $\alpha S_1$  emission from carbon nanodots exist in the literature, and most often these reported structures demonstrate  $\alpha S_1$  emission only after secondary fixation steps, a process by which bonds responsible for emission are rigidified, thereby reducing non-radiative transitions. This often requires incorporation into exterior frameworks [10,13,14], and therefore adds a layer of synthetic complexity. Herein we report a simple method for generating carbon nanodots that demonstrate excitation-dependent  $\alpha S_1$  in aqueous media.

Collection of the carbon nanodots was conducted using a combustion-based method that our lab has reported previously [7], and is also described by Scheme S1 in the supplementary material. Carbon nanodots were collected in water. After collection, single  $1 \times 1 \times 3$  cm cuvette experiments were conducted to characterize the photophysical properties of the carbon nanodots. Samples were transferred to a quartz cuvette, purged with either nitrogen or oxygen for one minute, then immediately analyzed. 2- and 3D steady state fluorescence spectra were collected using a FluoroMax 4-P spectrofluorometer; this same instrument was used for off-gated detection of alpha fluorescence with the following parameters: flash count, 100; time per flash (flash rate), 61 msec (16 Hz); flash delay, 0.05 msec; and sample window, 0.20 msec. Samples were thermally equilibrated at each temperature prior to analysis for ten to fifteen minutes using an equipped Peltier accessory. To complete single-cuvette Stern-Volmer studies, samples were thermally equilibrated in a quartz cuvette for fifteen minutes at the analysis temperature and then excited at relevant wavelengths. Quencher concentration was increased for each measurement by adding a very small volume of quencher solution to the sample cuvette and pumping to mix. Overall, < 5% of the original volume was added to the sample over the course of each experiment. Cycling experiments were performed on the FluoroMax 4-P, with one minute between cycles. Lifetime analysis was conducted with time-correlated single photon counting (TCSPC) instrumentation from Horiba Scientific and a NanoLED light source ( $\lambda_{ex} = 400$  nm,  $\lambda_{em} > 425$  nm). Impulse deconvolution of the fluorescence decays was completed using Decay Analysis Software v6.8. A multiexponential model (Eq. (1)) with a minimized  $\chi^2$  criterion was used, and values are reported as average lifetimes, calculated using Eqs. (2) and (3). For these equations  $\tau_i$  are the decay values,  $t$  is time,  $\alpha_i$  are the amplitudes, and  $\sum_i \alpha_i = 1$ .

$$I(t) = \sum_i \alpha_i \exp(-t/\tau_i) \quad (1)$$

$$f_i = \alpha_i \tau_i / \sum_i \alpha_i \tau_i \quad (2)$$

$$\bar{\tau} = \sum_i f_i \tau_i \quad (3)$$

Real-color photographs of luminescence emission were taken using a Nikon D7000 digital SLR camera. Samples were heated in quartz cuvettes to constant temperature, then were placed under a 405 nm laser and photographed. Temperatures were once again collected to ensure constant temperature. Cuvettes were also photographed in different orders to confirm that brightness differences were not due to inner filtering effects. Dynamic light scattering (DLS) measurements were taken using a Malvern Zetasizer Nano-ZS; samples were analyzed after shaking, sonication, and filtration through a 0.22  $\mu$ m pore.

Alpha fluorescence was first identified in these carbon nanodot samples by analyzing the 3D fluorescence spectra for carbon nanodots at 10 and 60  $^{\circ}$ C, as shown in Fig. S1 of the supplementary material. At 400 nm excitation, there is a significant enhancement in the fluorescence emission at higher temperatures (Fig. S2d). This stands in contrast to the emission at 240 nm excitation, which demonstrates a small signal decrease as temperature changes (Fig. S2a). Excitation at 270 and 330 nm were also plotted, as each of these wavelengths produces significant fluorescence for the sample (Fig. S2b and c); however, excitation at 270 produces two peaks which each have a different

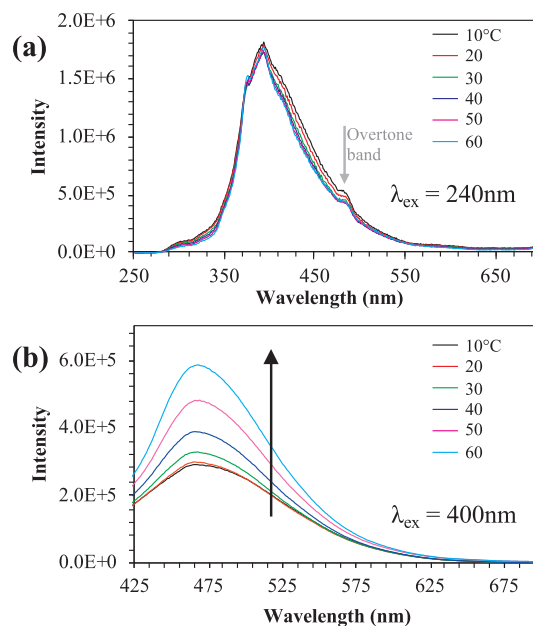


Fig. 1. Fluorescence spectra of carbon nanodots purged with nitrogen, with excitation wavelengths of (a) 240 nm and (b) 400 nm, analyzed at various temperatures ( $^{\circ}$ C).

response to temperature, implicating the possibility that 270 nm excitation yields emission from multiple fluorophores within the carbon nanodots. 330 nm excitation, meanwhile, only results in a slight fluorescence increase with temperature. Conversely, 400 nm excitation yielded a clear and significant response to temperature. As such, subsequent analysis of  $\alpha S_1$  from carbon nanodots was conducted at 400 nm excitation, using 240 nm excitation as a control. The 2D emission spectra for each of these excitation wavelengths are depicted in Fig. 1. While 240 nm excitation shows virtually no emission intensity changes as temperature is increased, emission due to 400 nm excitation demonstrates an overall 2-fold increase in intensity. In fact, the intensity at the maximum emission wavelength ( $\lambda_{max}$ ) for 400 nm excitation increases somewhat exponentially as a function of temperature (Fig. S3a). Classical fluorescence typically will demonstrate no change or an inverse relationship with increasing temperature, so the signal detected is likely due to a combination of prompt ( $S_1$ ) fluorescence and  $\alpha S_1$  emission, both occurring on different time scales. The observed increased intensity corresponds to a reduction in the full width half maximum (FWHM), indicating that as temperature is increased peak narrowing occurs. While this is observed also at 240 nm excitation, the FWHM reduction is more pronounced for 400 nm excitation where  $\alpha S_1$  is detected (Fig. S3b).

It is interesting to note also that  $\lambda_{max}$  is  $\sim 390$  nm and  $\sim 470$  nm for 240 and 400 nm excitation respectively. This indicates that different fluorophores within the carbon nanodots are responsible for emission at these wavelengths, as radiative decay generally results from the lowest energy excited state ( $S_1$ ). Thus, if one fluorophore were responsible for emission at both excitation wavelengths, 240 nm excitation would cause absorption to a higher electronic level ( $S_0 \rightarrow S_n$ ) that would subsequently decay to the  $S_1$  state before emitting. Were this the case, we would expect to detect a single  $\lambda_{max}$  irrespective of excitation wavelength; this is not observed, implicating the presence of multiple fluorophores in the carbon nanodot structures. The absorption spectra of the carbon nanodots additionally suggests the presence of multiple fluorophores, as broad absorption is observed from 200 to 600 nm wavelengths (Fig. S4). This multi-fluorophore phenomenon has also been probed previously by our lab using fluorescence quenchers and Stern-Volmer analysis [16]. Using a carbon nanodot sample at room temperature, quenching effects from concentrations of bromide ion

(Br<sup>-</sup>) from sodium bromide, cesium ion (Cs<sup>+</sup>) from cesium chloride, and acrylamide quenchers were studied at the excitation maximum of 334 nm (Fig. S5). While both the bromide and cesium ions exhibited linear quenching trends, the acrylamide-quenched data exhibited positive deviation towards the x-axis (Fig. S5a). This non-linear trend is frequently indicative of multiple fluorophores with varied accessibility to the quencher; this is further supported by the loss of vibronic structure observed for the acrylamide-quenched spectra in Fig. S5b of the supplementary material. Observation of this structure in the original spectrum could suggest that fluorophores are buried within the carbon nanodot core; only after acrylamide diffuses into the core is vibronic structure lost [16]. Having observed this for fluorescent carbon nanodots alone, we additionally completed Stern-Volmer analysis for 240 and 400 nm excitations, which will be discussed in more detail in later sections.

Having detected distinct fluorophores at 240 and 400 nm excitation wavelengths, we subsequently investigated the nature of these signals, as different decay transitions (including intersystem crossing) may be possible for different fluorophores within the carbon nanodots. To confirm that increased intensity for  $\lambda_{\text{ex}} = 400$  nm is due to  $\alpha\text{S}_1$  emission, spectra were collected using off-gated parameters, which permit only the detection of long-lived ( $> 10^{-6}$  sec) signals, Fig. 2b. The trends for these data correspond to those observed during the steady state collection (where both  $\text{S}_1$  and  $\alpha\text{S}_1$  are detected), implicating the  $\alpha\text{S}_1$  state as a significant source of overall emission. When considering excitation at 240 nm, it is interesting to note that the overall off-gated emission intensity has decreased by an order of magnitude relative to steady state collection, and it is likely, therefore, that this signal is only detected due to residual excitation from the source lamp decay. Intensity from 400 nm excitation under off-gated parameters, however, has actually increased by approximately 60% relative to the steady state emission, indicating that  $\alpha\text{S}_1$  fluorescence is a significant radiative pathway for the carbon nanodots when excited at this wavelength.

This signal is more efficiently detected using off-gated parameters, demonstrating the long-lived nature of the emission, thus implicating  $\alpha\text{S}_1$  fluorescence. When comparing the normalized spectra for both steady state and off-gated detection methods (Fig. S6), there is no variation in spectral shape or position at 240 nm excitation for both methods at either 10 or 60 °C. This confirms that the signal arises from

the same set of singlet excited states for both detection methods. Similarly, at 400 nm excitation,  $\lambda_{\text{max}}$  remains the consistent between methods. This long-lived signal can therefore be described as  $\alpha\text{S}_1$  fluorescence rather than phosphorescence. For direct  $\text{T}_1 \rightarrow \text{S}_0$  transitions, the resulting emission is commonly red-shifted, as excited triplet states are generally lower in energy than excited singlet states. Alpha fluorescence, conversely, is the result of RISC to the original singlet excited state prior to emission, so no shift in peak wavelength is expected. At 400 nm excitation, however, the off-gated emission is narrower than its steady state counterpart at 60 °C (Fig. S6d). Under steady state conditions, where both  $\alpha\text{S}_1$  and prompt  $\text{S}_1$  emission are detected, narrowing was observed at higher temperatures while the signal intensity increased (Fig. S7); the decrease in FWHM is more pronounced for 400 nm excitation under off-gated collection parameters, where  $\alpha\text{S}_1$  is dominant, implying that this narrowing is due to interactions specific to  $\alpha\text{S}_1$ . This stands in contrast to 240 nm excitation, where some peak narrowing is observed with virtually no change in integrated intensity (Fig. S8). Since the same prompt fluorescence signal is detected at 240 nm excitation in both steady state and off-gated detection methods, it follows that there should be no difference in spectral shape or position from each detection method, which is in fact observed (Fig. S6a/b).

It is noteworthy that  $\alpha\text{S}_1$  is observable under our synthesis conditions, as previous reports required additional fixation prior to detection [10,13,14]. Additionally,  $\alpha\text{S}_1$  was not observable in our carbon nanodot samples analyzed immediately after synthesis. To understand how these  $\alpha\text{S}_1$  structures might differ from other carbon dots reported in literature, DLS was performed to obtain size information, shown in Fig. 3. After simply shaking the solution, DLS interestingly reported dominant particle sizes of  $80 \pm 20$  nm, which stands in contrast to previous reports from our lab of  $\sim 1$  nm particles for carbon nanodot structures [7].

The sample was sonicated, and a similar size reporting was observed, but with an improved polydispersity index (0.430→0.223). Upon filtration to remove larger particles, however, the dominant peak became  $\sim 1$  nm. When allowed to stand, the peaks detected for the filtered solution began to shift to larger sizes (Fig. 3c), indicating possible aggregation. Interestingly, the peak at 100 nm became more dominant by volume after this standing period. When both the shaken and filtered solutions were excited at 400 nm from 10 to 60 °C, the initial solution maintained  $\alpha\text{S}_1$  properties (Fig. S9a), while the filtered solution did not (Fig. S9b). Interestingly, both the initial and filtered spectra are similar in shape when normalized at 10 °C (Fig. S9c). This indicates that potential aggregation does not have an effect on emission properties for 400 nm at low temperatures where  $\alpha\text{S}_1$  is unlikely to occur; thus, properties of the carbon nanodots can be preserved despite aggregation. It is possible, therefore, that the carbon nanodots are able to self-fixate bonds responsible for the  $\alpha\text{S}_1$  emission and thus the signal becomes detectable in aqueous solution.

This phenomenon can be further discussed in relation to the Stern-Volmer analysis mentioned previously. Using an alpha-fluorescent carbon nanodot sample, we performed quenching experiments using bromide ion and acrylamide at 60 °C using off-gated detection parameters. Under these conditions,  $\alpha\text{S}_1$  is more readily detected, permitting the Stern-Volmer data to more closely reflect  $\alpha\text{S}_1$  specifically. As shown in Fig. 4a, quenching from bromide ion is particularly significant for 400 nm excitation where  $\alpha\text{S}_1$  is detected; however, essentially no significant quenching is reported for 240 nm excitation. We have shown carbon nanodots to exhibit surface charges previously using gel electrophoresis [unpublished data]; therefore, it is possible that suitably high concentrations of bromide ion could saturate surface charge interactions and thus permit diffusion of the ions into the carbon nanodot core. As aggregation is likely the result of intermolecular forces such as hydrogen bonding or dipole-dipole interactions, bromide ions could disrupt these forces within the carbon nanodot aggregates. As such, bromide quenchers could de-stabilize the bonds responsible for alpha fluorescence, leading to a more notable quenching response than either

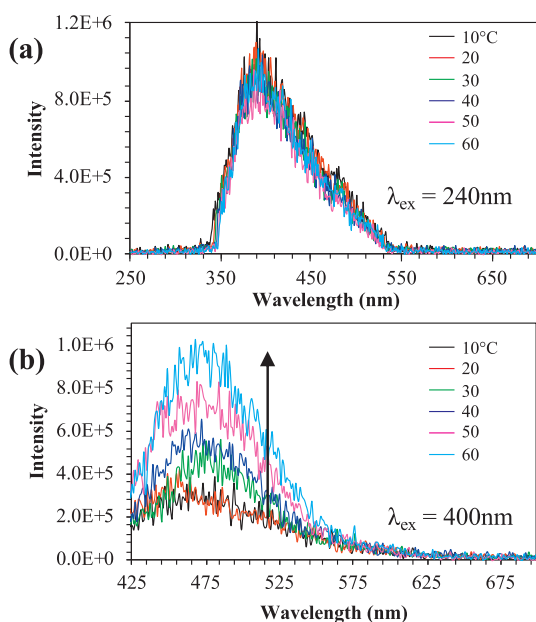
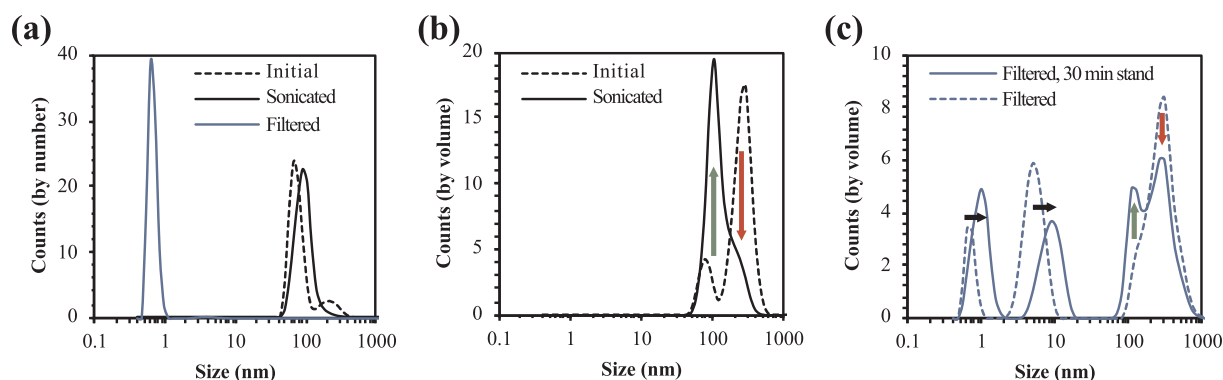
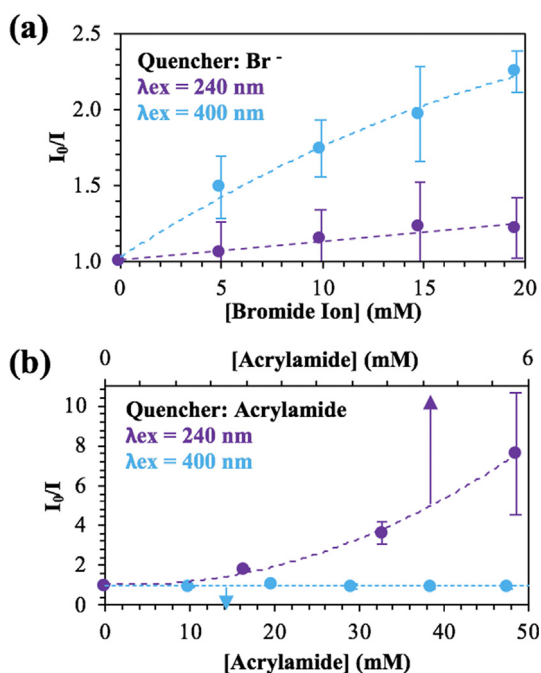


Fig. 2. Off-gated (delayed) collection of fluorescence spectra of carbon nanodots purged with nitrogen, with excitation wavelengths of (a) 240 nm and (b) 400 nm, analyzed at various temperatures.



**Fig. 3.** Diameter of carbon nanodots after mixing (initial), sonication, and filtration, as analyzed by dynamic light scattering. Size distributions are reported (a) by number, (b) by volume of the initial sample before and after sonication, and (c) by volume of the filtered sample for 0 (filtered) and 30 min (filtered, 30 min stand) after filtration.



**Fig. 4.** Stern-Volmer plots of carbon nanodots at 60 °C with excitation wavelengths of 240 and 400 nm, using an off-gated detection method. Quenchers used include (A) bromide ion from sodium bromide and (B) acrylamide. Error is standard deviation from three independent trials.

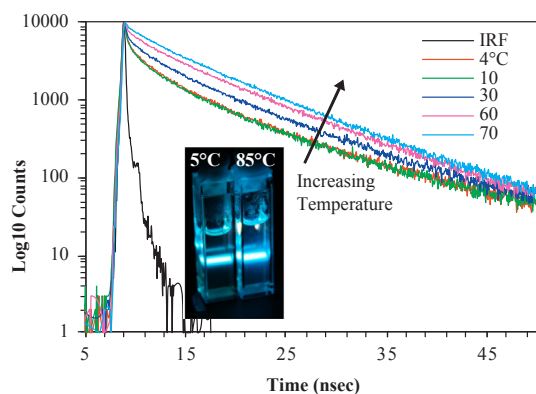


**Fig. 5.** Time-resolved intensity decay curves of carbon nanodots purged with nitrogen ( $\lambda_{\text{ex}} = 400 \text{ nm}$ ,  $\lambda_{\text{em}} = 460 \text{ nm}$ ) collected over various temperatures. *Inset.* Photographs of samples at both 5 °C and 85 °C, excited with a 405 nm laser. Photograph demonstrates the increased brightness of the sample at 85 °C.

a static or dynamic mechanism alone. In fact, when comparing quenching effects at 400 nm excitation to those reported from bromide ion at 240 nm excitation, the carbon nanodots are demonstrably more sensitive to quenching when alpha fluorescence is a dominant radiative pathway (Fig. 4a, S10).

We also observed the response of fluorescence at these excitation wavelengths to a neutral acrylamide quencher (Fig. 4b, S11). Interestingly, emission at 240 nm excitation demonstrates a biphasic trend, deviating away from the x-axis at higher concentrations. This likely indicates both the presence of static and dynamic quenching mechanisms for this emission. What is of particular note, however, is the lack of quenching response from 400 nm excitation, shown by a linear trend exhibiting a slope of zero. This is observed even at concentrations that are nearly 10-fold those used to quench emission from 240 nm excitation. This could potentially reinforce the concept of bond fixation from aggregation, as a neutral quencher would be unable to interrupt the intermolecular forces from charged or partially charged interacting species to produce a similar response as is observed for bromide ions.

To further investigate the potential alpha-fluorescent character of emission from 400 nm excitation, we subsequently assessed the impact of an oxygen-saturated solution on emission. Given that triplet states are also typically readily quenched by molecular oxygen due to longer lifetimes and favorable triplet-triplet interactions, samples were purged with oxygen and analyzed. As shown in Fig. S12 of the supplementary material, when analyzing a sample purged with oxygen the trends in emission intensity and FWHM have changed compared to the nitrogen purged samples. Although emission still increases when excited at 400 nm, the percent increase is lower than that of the sample purged with nitrogen. Molecular oxygen readily quenches excited triplet states, preventing back intersystem crossing and subsequently  $\alpha S_1$  fluorescence. This reduces the overall contribution from  $\alpha S_1$  to the steady state detected fluorescence emission. At 240 nm excitation, conversely, there is little change in the trend of percent signal increase, and fluorescence still has an overall net decrease at higher temperatures. The effects of oxygen on  $\alpha S_1$  fluorescence quenching can also be observed in the values of FWHM, which we have previously observed to decrease for  $\alpha S_1$  emission and for  $S_1$  emission at 400 nm and 240 nm excitations respectively. Excitation at 240 nm produces statistically comparable lines of best fit for the decrease in FWHM for both the nitrogen and oxygen purged samples (Figs. S3b and S12b). This implies that oxygen quenching plays no role in the emission distribution for excitation at 240 nm, where there is no  $\alpha S_1$  fluorescence detected. Both fits have  $R^2$  values that approach 1 ( $> 0.96$ ) and have residual values evenly distributed about zero, indicating the suitability of a linear model. Excitation at 400 nm is also sufficiently fit by a linear model when purged with nitrogen (Fig. S3b,  $R^2 = 0.9938$ ). This stands in contrast to the oxygen-purged sample (Fig. S12b), which has an  $R^2$  value 0.8871 and diverging residuals. This indicates that these data are not suitably

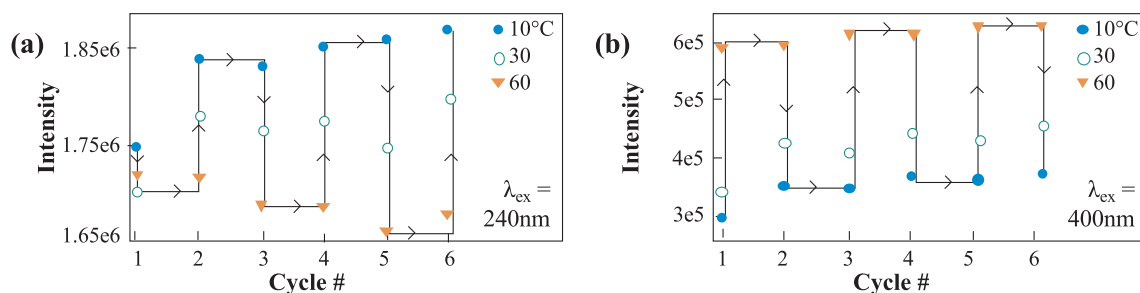


**Fig. 6.** During temperature cycling, fluorescence spectra of carbon nanodots purged with nitrogen with excitation wavelengths of (a) 240 nm and (b) 400 nm, are analyzed at various temperatures. Intensities are reported from emission  $\lambda_{max}$ .

described by a linear model, and instead show little peak narrowing until 40 °C when there is a sudden sharpening of emission. A similar trend is observed in the percent signal increase of the same sample. At lower temperatures,  $\alpha S_1$  contributes less to the overall emission, as it is an unfavorable radiative process under these conditions. With oxygen available to quench the excited triplet states, it is even less likely that the detected emission at lower temperatures will contain a significant contribution from  $\alpha S_1$ . Subsequently, until  $\alpha S_1$  emission becomes a dominant radiative pathway, the trend of decreasing FWHM is not observed strongly, even in comparison to the decrease between 0 and 40 °C of the nitrogen purged sample (Fig. S3b). Once  $\alpha S_1$  is dominant (> 40 °C), however, the trend in FWHM begins to match that which was observed for the nitrogen purged sample, where quenching of the triplet state is less of a factor. Although these trends in emission intensity and FWHM are noted, the magnitude of observed changes is relatively minimal. This would be expected if bond fixation from aggregation is responsible for detectable alpha fluorescence, as this system would also protect the fluorophores from quenching due to oxygen, similar to the previously discussed trends from acrylamide quenching.

Fluorescent lifetimes at 400 nm excitation were then analyzed to determine the effect of heating. As shown in Fig. 5, at lower temperatures the fluorescence emission decays appear multi-exponential.

As previously discussed, carbon nanodots are known to contain a multitude of fluorophores that can contribute to emission; each of these may have different lifetimes due to different radiative and non-radiative decay rates. As the temperature is increased, however, the decays appear mono-exponential. This implies that at higher temperatures, there is less detected fluorescence from multiple emission sources. This could be due to a higher incidence of transition from the  $S_1 \rightarrow T_1$  state for the alpha fluorescent fluorophore(s), competitive to photonic emission and subsequent detection during nanosecond lifetime analysis. This is further supported by examining the average fluorescence lifetimes for carbon nanodot samples at these temperatures, as shown in Fig. S13 of the supplementary material (fitting parameters in Figs. S14 and S15). When the samples are purged with nitrogen, there is a linear decrease in lifetime from 7.5 to 7.0 nsec as the temperature is raised from 10 to 60 °C. The lifetime is calculated by using Eq. (4), where  $k_{nr}$  are the decay rates of all non-radiative processes and  $\Gamma$  is the radiative decay rate.

$$\tau = 1/(\Sigma k_{nr} + \Gamma) \quad (4)$$

As the temperature is increased, ISC and RISC become more favorable; however, RISC occurs on a much longer time scale than is detected during fluorescence lifetime analysis. As such, the intersystem crossing rate from the  $S_1 \rightarrow T_1$  transition may increase while the emissive radiative decay rate stays constant, lowering the overall lifetime. A decrease of 0.6 nsec is also observed in the oxygen-purged samples from 10 to 60 °C; however, the decrease in lifetime occurs more rapidly as the temperature is raised. This can be attributed to the simultaneous increase of non-radiative decay rates from  $S_1 \rightarrow T_1$  ( $k_{nr,S_1 \rightarrow T_1}$ ) and quenching from molecular oxygen ( $k_{nr,O}$ ). As temperature increases, oxygen diffuses more readily and can therefore more rapidly quench

excited states.

We subsequently questioned whether the carbon nanodot samples would be stable over multiple cycles of both heating and cooling, which would be a vital requirement for any potential future  $\alpha S_1$  probe. As shown in Fig. 6, both 240 and 400 nm excited samples demonstrate no net decrease in fluorescence emission over time, indicating that the probe is likely not photobleaching over multiple excitation-emission event cycles. At lower temperatures the fluorescence emission intensity, when excited at 240 nm, appears to actually slightly increase; however, the overall net increase is only ~2% while the decrease detected at 60 °C at this excitation wavelength is even lower. Excitation at 400 nm displays no decrease in emission intensity over 6 excitation-emission event cycles, indicating that the carbon nanodots are also thermally stable and could therefore be employed as potential  $\alpha S_1$  probes.

In closing, we have reported the detection of  $\alpha S_1$  emission from carbon nanodots collected into water via a combustion-based synthesis strategy. This low-cost and facile synthesis yields nanoparticles that demonstrate temperature-dependent  $\alpha S_1$  fluorescence emission, with possible detection likely due to aggregation of synthesized carbon nanodots. Emission from both  $S_1$  and  $\alpha S_1$  are shown to be both thermally stable and photostable, with a reduction in average fluorescent lifetime as intersystem and reverse intersystem crossing become more favorable. This report sets the foundation for the potential future use of carbon nanodots as alpha fluorescence probes in aqueous media.

#### Declaration of interests

The authors declare that they have no known competing financial interests or personal relationships that could have appeared to influence the work reported in this paper.

#### Acknowledgements

The authors acknowledge the Institute of Fluorescence (IoF) as well as the Department of Chemistry and Biochemistry at the University of Maryland Baltimore County (UMBC) for financial support. The authors would also like to thank the lab of Dr. Marie-Christine Daniel for assistance with dynamic light scattering measurements.

#### Appendix A. Supplementary material

Supplementary data to this article can be found online at <https://doi.org/10.1016/j.cplett.2019.02.039>.

#### References

- [1] I.Y. Goryacheva, A.V. Sapelkin, G.B. Sukhorukov, *TrAC Trends Anal. Chem.* 90 (2017) 27.
- [2] M. Shamsipur, A. Barati, S. Karami, *Carbon* 124 (2017) 429.
- [3] G. Hong, S. Diao, A.L. Antaris, H. Dai, *Chem. Rev.* 115 (2015) 10816.
- [4] F. Yuan, S. Li, Z. Fan, X. Meng, L. Fan, S. Yang, *Nano Today* 11 (2016) 565.
- [5] H. Li, H. Ming, Y. Liu, H. Yu, X. He, H. Huang, K. Pan, Z. Kang, *New J. Chem.* 35 (2011) 2666.

- [6] L. Haitao, K. Zhenhui, L. Yang, L. Shuit-Tong, *J. Mater. Chem.* 22 (2012) 24230.
- [7] R. Knoblauch, B. Bui, A. Raza, C.D. Geddes, *Phys. Chem. Chem. Phys.* 20 (2018) 15518.
- [8] S. Tao, S. Lu, Y. Geng, S. Zhu, S.A.T. Redfern, Y. Song, T. Feng, W. Xu, B. Yang, *Angew. Chem.* 130 (2018) 2417.
- [9] Q. Li, M. Zhou, M. Yang, Q. Yang, Z. Zhang, J. Shi, *Nat. Commun.* 9 (2018) 734.
- [10] J. Liu, N. Wang, Y. Yu, Y. Yan, H. Zhang, J. Li, J. Yu, *Sci. Adv.* 3 (2017) e1603171.
- [11] S. Sarkar, D. Gandla, Y. Venkatesh, P. Bangal, S. Ghosh, Y. Yang, S. Misra, *Graphene Quantum Dots from Graphite by Liquid Exfoliation Showing Excitation-Independent Emission, Fluorescence Upconversion and Delayed Fluorescence*, Royal Society of Chemistry, Great Britain, 2016, p. 21278.
- [12] J. Hou, L. Wang, P. Zhang, Y. Xu, L. Ding, *Facile Synthesis of Carbon Dots in An Immiscible System with Excitation-Independent Emission and Thermally Activated Delayed Fluorescence*, Royal Society of Chemistry, Great Britain, 2015, p. 17768.
- [13] J. He, Y. He, Y. Chen, X. Zhang, C. Hu, J. Zhuang, B. Lei, Y. Liu, *Chem. Eng. J.* 347 (2018) 505.
- [14] J. Kai, W. Yuhui, C. Congzhong, L. Hengwei, *Chem. Mater.* 29 (2017) 4866.
- [15] N.J. Turro, *Modern Molecular Photochemistry*, University Science Books, Mill Valley, Calif., 1991.
- [16] R. Schmitz, *Synthesis, Characterization, and Plasmonic Enhancement of Fluorescent Carbon Nanodots*, Ph.D. Diss. University of Maryland Baltimore County, ProQuest, 2016.